iScience

CellPress
OPEN ACCESS

Article

Control of epigenomic landscape and development of fetal male germ cells through L-serine metabolism

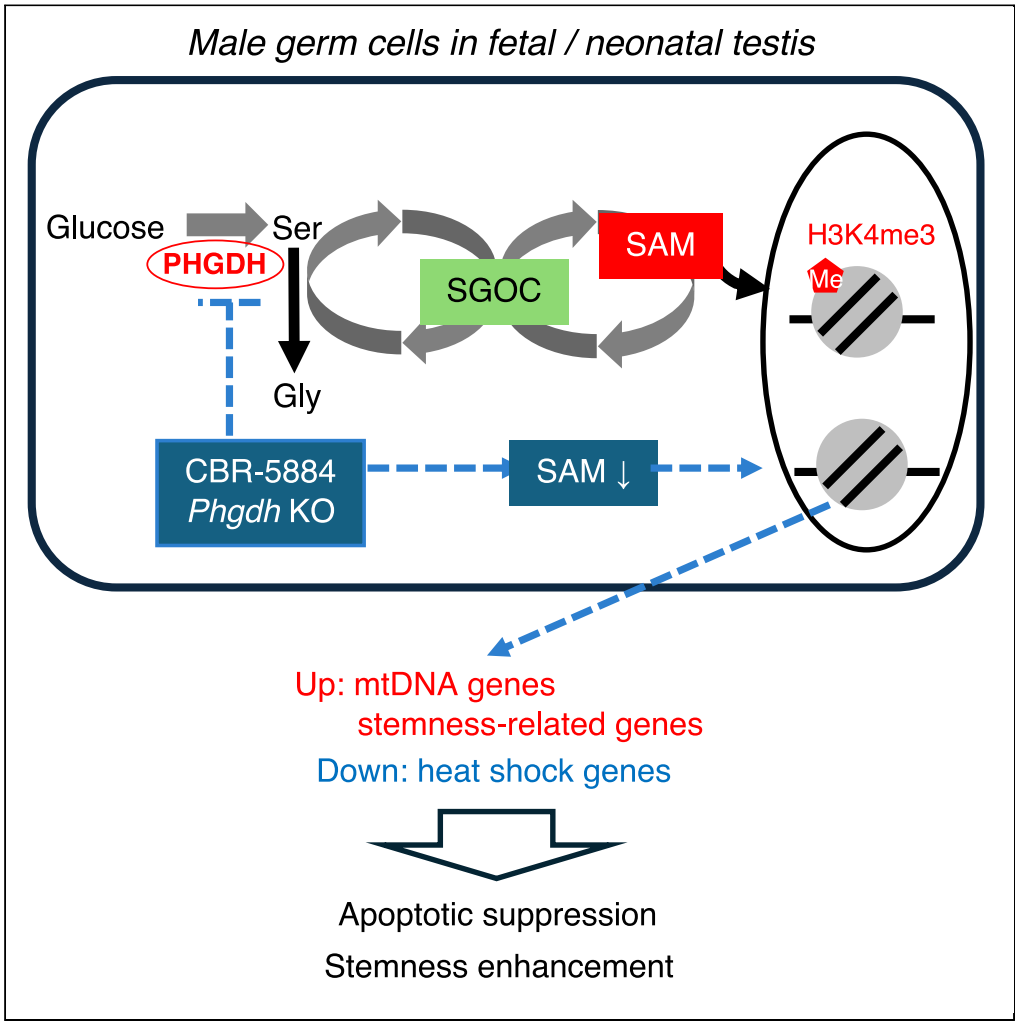

Yohei Hayashi, Jintaro Kaneko, Yumi Ito-Matsuoka, ..., Kenjiro Shirane, Shigeki Furuya, Yasuhisa Matsui

yohei.hayashi.e2@tohoku.ac.jp (Y.H.)
yasuhisa.matsui.d3@tohoku.ac.jp (Y.M.)

Highlights

PHGDH and SAM levels increase during fetal germ cell differentiation in testes

PHGDH inhibition reduces SAM and alters germline gene expression in testes

PHGDH inhibition disrupts the germline epigenome, but SAM complements this effect

This regulatory mechanism controls germ cell numbers and stemness in spermatogonia

Hayashi et al., iScience 27, 110702
September 20, 2024
https://doi.org/10.1016/j.isci.2024.110702

iScience

CellPress
OPEN ACCESS

Article

Control of epigenomic landscape and development of fetal male germ cells through L-serine metabolism

Yohei Hayashi,[1,2,3,*] Jintaro Kaneko,[4] Yumi Ito-Matsuoka,[1] Asuka Takehara,[1] Mayuka Funakoshi,[5] So Maezawa,[5] Kenjiro Shirane,[6] Shigeki Furuya,[7] and Yasuhisa Matsui[1,2,3,8,*]

SUMMARY

Sex-specific metabolic characteristics emerge in the mouse germ line after reaching the genital ridges around embryonic day 10.5, coinciding with sexual differentiation. However, the impact of such metabolic characteristics on germ cell development remains unclear. In this study, we observed the specific upregulation in male fetal germ cells of D-3-phosphoglycerate dehydrogenase (PHGDH), the primary enzyme in the serine-glycine-one-carbon metabolism, along with an increase in a downstream metabolite, S-adenosylmethionine (SAM), crucial for protein and nucleic acid methylation. Inhibiting PHGDH in fetal testes resulted in reduced SAM levels in germ cells, accompanied by increases in the number of mouse vasa homolog (MVH/VASA)-positive germ cells and the promyelocytic leukemia zinc finger (PLZF)-positive undifferentiated spermatogonia ratio. Furthermore, PHGDH inhibition led to a decrease in the methylation of histone H3 and DNA, resulting in aberrations in gene expression profiles. In summary, our findings underscore the significant role of certain metabolic mechanisms in the development of male germ cells.

INTRODUCTION

In mice, primordial germ cells (PGCs), which are precursors to both spermatozoa and oocytes, migrate to the genital ridges around embryonic day (E) 10.5.[1] During this migration, global erasure of existing DNA methylation in PGCs occurs, resulting in an overall methylation reduction to <10% by E13.5.[2] Concurrently, the sexual fate of germ cells is shaped by factors secreted by gonadal somatic cells, leading to initiation of sex determination around E10.5.[3] After sex determination, male germ cells, known as gonocytes or prospermatogonia, undergo cycles of proliferation and apoptosis and enter mitotic arrest in the G0/G1 phase around E14.5–E15.5.[4,5] Active proliferation resumes on approximately postpartum day (P) 5, with certain cells differentiating into spermatogonial stem cells (SSCs).[6] In contrast, female germ cells commence meiosis around E13.5, progressing through meiosis and eventually arresting at prophase I (diplotene stage) within neonatal ovaries.[7]

Metabolic processes are essential not only for energy production and the synthesis of cellular building blocks but also for the regulation of various cell functions and differentiation. Our prior proteomic and metabolomic studies revealed that the acquisition of sex-specific metabolic characteristics in fetal germ cells occurs shortly after sexual differentiation.[8,9] Notably, in male fetal germ cells, the tricarboxylic acid (TCA) cycle and Ser-Gly-one-carbon (SGOC) metabolism, which encompass L-serine and L-glycine biosynthesis, the folate cycle, and the methionine cycle, are continually upregulated in comparison to fetal female germ cells (Figure S1). Conversely, oxidative phosphorylation through pyruvate and fatty acid metabolism is upregulated in the female germ line, indicating sexual differences in substrate reliance for energy metabolism in fetal germ cells.

In females, inhibition of fatty acid metabolism leads to a significant reduction in the number of germ cells through activation of the p53 pathway around E11.5–E13.5.[10] By comparison, inhibiting pyruvate uptake by mitochondria in fetal mouse ovaries results in a suppression of early folliculogenesis, which can be attributed to the downregulation of transforming growth factor β-related genes crucial for folliculogenesis.[11] Although details are becoming clearer regarding the regulatory mechanisms through which upregulation of metabolic pathways in the

[1]Cell Resource Center for Biomedical Research, Institute of Development, Aging and Cancer (IDAC), Tohoku University, 4-1 Seiryo-machi, Aoba-ku, Sendai, Miyagi 980-8575, Japan
[2]Graduate School of Life Sciences, Tohoku University, 2-1-1 Katahira, Aoba-ku, Sendai, Miyagi 980-8577, Japan
[3]Graduate School of Medicine, Tohoku University, 2-1 Seiryo-machi, Aoba-ku, Sendai, Miyagi 980-8575, Japan
[4]School of Medicine, Tohoku University, 2-1 Seiryo-machi, Aoba-ku, Sendai, Miyagi 980-8575, Japan
[5]Department of Applied Biological Science, Faculty of Science and Technology, Tokyo University of Science, Yamazaki 2641, Noda, Chiba 278-8510, Japan
[6]Department of Genome Biology, Graduate School of Medicine, Osaka University, 2-2 Yamadaoka, Suita, Osaka 565-0871, Japan
[7]Department of Bioscience and Biotechnology, Graduate School of Bioresource and Bioenvironmental Sciences, Kyushu University, 744 Motooka, Fukuoka 819-0395, Japan
[8]Lead contact
*Correspondence: yohei.hayashi.e2@tohoku.ac.jp (Y.H.), yasuhisa.matsui.d3@tohoku.ac.jp (Y.M.)
https://doi.org/10.1016/j.isci.2024.110702

female germ line influences germ cell differentiation, the corresponding mechanisms through which metabolic pathways upregulated in the male germ line affects male germline differentiation remain unknown.

Remarkably, recent research has revealed connections between the metabolic pathways upregulated in fetal male germ cells, specifically the TCA cycle and SGOC metabolism, and epigenetic regulation.[12,13] For instance, histone acetyltransferases depend on acetyl-coenzyme A, a metabolite associated with the TCA cycle, as the substrate for donating acetyl groups.[14] Additionally, various TCA cycle-related metabolites, namely alpha-ketoglutarate, succinate, and fumarate, are involved in regulating histone methyltransferases of the jumonji C domain-containing demethylase class, as well as members of the ten-eleven translocation DNA demethylase family.[15] Conversely, both histone methyltransferases and DNA methyltransferases (DNMTs) rely upon S-adenosylmethionine (SAM), a metabolite synthesized via the SGOC pathway, as a methyl-donor substrate. These insights suggest that the upregulation of these metabolic pathways plays a role in regulating the epigenomic reorganization observed in the male fetal germ line. However, the significance of this relationship remains to be fully elucidated.

Building upon our earlier discoveries, the current investigation revealed a transient elevation in the expression of D-3-phosphoglycerate dehydrogenase (PHGDH), the pivotal enzyme governing SGOC metabolism, and a concomitant increase in SAM levels within male fetal germ cells. Disruption of germline PHGDH function via either pharmacological inhibition or conditional knockout (KO) led to reductions in histone H3 and DNA methylation, induced alterations in the expression of stemness-associated genes, and exerted discernible effects on the survival and differentiation of germ cells in fetal testes. These analyses provide insights into potential mechanisms through which SGOC-mediated regulation affects fetal male germ cell development.

RESULTS

Changes in SGOC metabolism during germline differentiation

In our previous investigation, we noted that several enzymes and metabolites involved in SGOC metabolism in male germ cells were upregulated at E13.5 relative to females.[9] In the present study, we explored the developmental stage-dependent changes in the levels of these enzymes and metabolites (Figure 1). In both sexes, expression of the rate-limiting enzyme in SGOC metabolism, PHGDH (Figure 1A), was significantly reduced in germ cells compared with somatic cells at E12.5. Nevertheless, a marked upregulation was observed in male germ cells at E16.5 compared with the expression level in testicular somatic cells at the same fetal stage (Figures 1B and 1C). The relatively elevated expression of PHGDH in germ cells compared with somatic cells persisted in the testes at P1 and P7, although to a lesser extent at P7 than E16.5 (Figures S2A and S2B). These findings suggest L-serine metabolism is activated specifically in male germ cells following sexual differentiation.

To elucidate the impact of increased PHGDH expression on metabolite levels, we examined fluctuations in the levels of key metabolites in the SGOC pathway during germ cell differentiation. Given the involvement of SGOC metabolism in the synthesis of SAM, a substrate for methylation reactions and contributor to epigenetic regulation (Figure 1D), we assessed SAM levels during fetal germ cell differentiation using immunostaining with anti-SAM antibodies (Figure 1E). The results revealed that, similar to PHGDH, SAM intensity varied minimally in E12.5 germ cells compared with surrounding somatic cells in both sexes (Figure 1F). However, at E16.5, a specific increase in the SAM level was observed in male germ cells, which persisted at P1 and P7 compared with somatic cells of the same fetal stage, although to a lesser degree than at E16.5. These observations suggest that male germ cell-specific enhancement of SGOC metabolism and its associated metabolites occurs following sexual differentiation.

Effects of PHGDH inhibition in fetal testicular organ culture

To elucidate the impact of the upregulation of SGOC metabolism observed in male germ cells, we investigated the effects of PHGDH inhibition using organ cultures of E12.5 testes. The differentiation of germ cells into spermatogonia can be facilitated using gas-liquid interphase culture of fetal testes (Figure 2A).[16] In this culture system, a tubular structure resembling seminiferous tubules develops, with VASA-positive germ cells localized within the tubular structure (Figures 2B and 2C). Addition of the PHGDH inhibitor CBR-5884 (CBR) (Figure 1A) resulted in an increase in the number of VASA-positive germ cells and promyelocytic leukemia zinc finger (PLZF)-positive undifferentiated spermatogonia in the cultured testes at day 14 (Figures 2D and 2E). CBR-5884 treatment also led to an increase in the ratio of PLZF-positive spermatogonia among VASA-positive germ cells, indicating that PHGDH suppression promotes an increase in the number of germ cells, especially undifferentiated spermatogonia (Figure 2F). Conversely, the addition of CBR-5884 to fetal ovarian cultures did not inhibit follicle formation or growth nor result in any morphological differences (Figure S2E). These findings suggest that PHGDH function is not crucial for oogenesis during the fetal to neonatal period.

To elucidate the impact of PHGDH inhibition on SAM synthesis, we analyzed SAM levels in VASA-positive germ cells of organ culture testes at day 14 (Figure 2G). Inhibition of PHGDH resulted in a decrease in SAM levels in VASA-positive germ cells relative to somatic cells (Figure 2H). Furthermore, addition of SAM to the culture medium suppressed the increase in VASA-positive germ cells and PLZF-positive undifferentiated spermatogonia (Figures 2I and 2J) and diminished the ratio of undifferentiated spermatogonia in cultured testes to the same level as that observed in cultured testes treated with dimethyl sulfoxide (DMSO) alone (Figure 2K). Conversely, the supplementation of L-serine, a direct downstream metabolite of PHGDH, did not complement the changes induced by CBR addition (Figures S2F–S2I). This may be attributed to the role of L-serine as an activator of pyruvate kinase 2 (PKM2) within the glycolytic pathway, which subsequently causes further inhibition of the influx of glucose-derived carbon into serine biosynthesis.[17] This result suggests that the male germ cell-specific increase in SAM levels depends on an increase in PHGDH expression and negatively affects the ratio of undifferentiated spermatogonia in cultured testes.

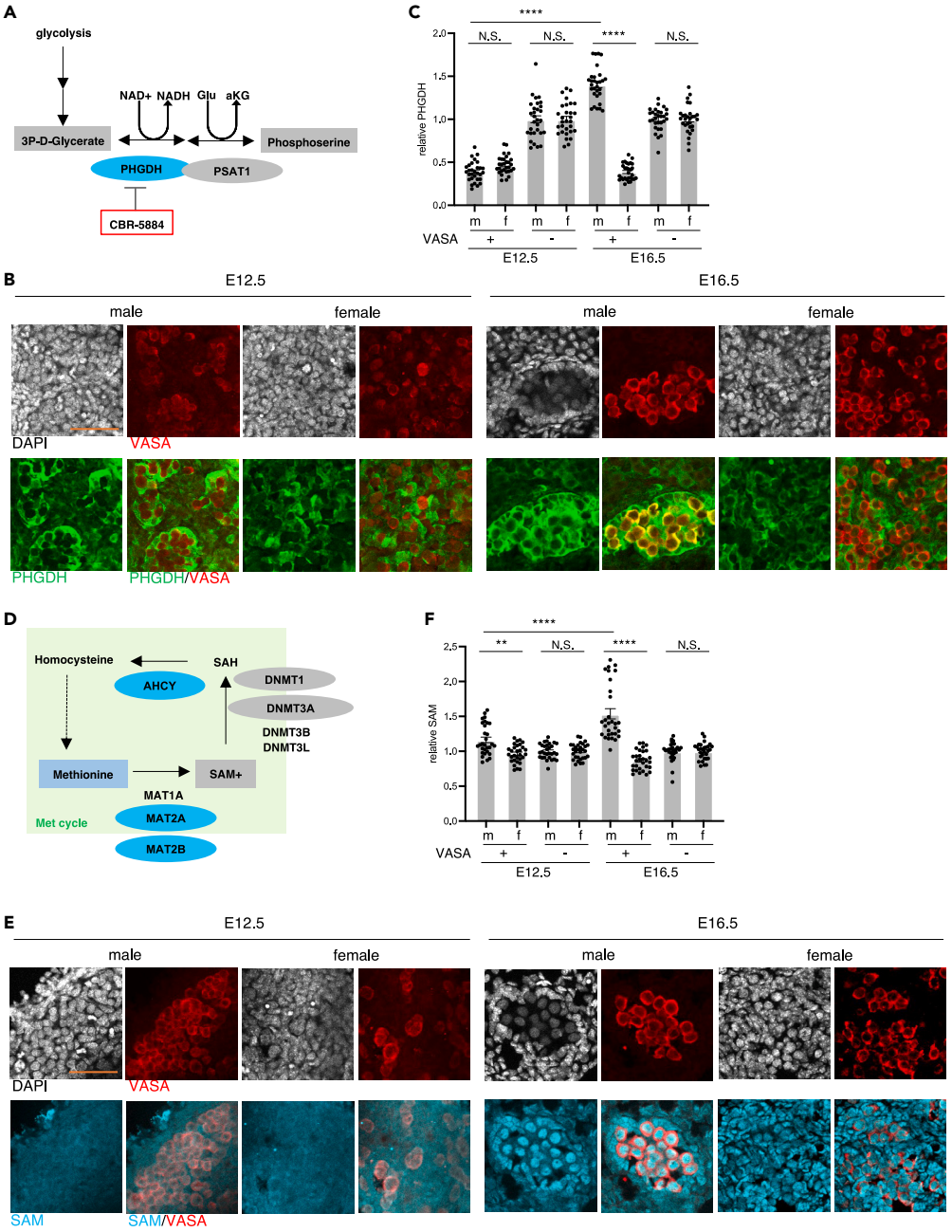

Figure 1. Changes in SGOC metabolism during germline differentiation

(A) Schematic representation of metabolic pathways around PHGDH. Cyan denotes components more abundant in male germ cells than female germ cells.

(B) Immunostaining analysis depicting changes in PHGDH expression during fetal germline differentiation. Testes and ovaries were examined at E12.5 and E16.5.

(C) Quantification of relative fluorescence signal intensity of PHGDH in VASA-positive germ cells and surrounding somatic cells in fetal gonads (total of 29–30 cells from three biological replicates). Graphs present relative fluorescence intensity, with the fluorescence intensity of VASA-negative somatic cells at each fetal age set as 1.

(D) Schematic illustration of metabolic pathways around SAM. Cyan indicates components more abundant in male germ cells than female germ cells.

(E) Immunostaining analysis revealing changes in SAM abundance during fetal germline differentiation. Testes and ovaries were examined at E12.5 and E16.5.

(F) Quantification of relative fluorescence signal intensity of SAM in VASA-positive germ cells and surrounding somatic cells in fetal gonads (total of 30 cells from three biological replicates). Graphs present relative fluorescence intensity, with the fluorescence intensity of VASA-negative somatic cells at each fetal age set as 1. Data information: values represent mean ± SE of three independent experiments. Statistical significance indicated as N.S. (not significant), $^{**}p < 0.01$, $^{****}p < 0.0001$ (one-way ANOVA and Tukey's multiple comparisons test). Scale bar: 50 μm.

Refer also to Figures S1 and S2.

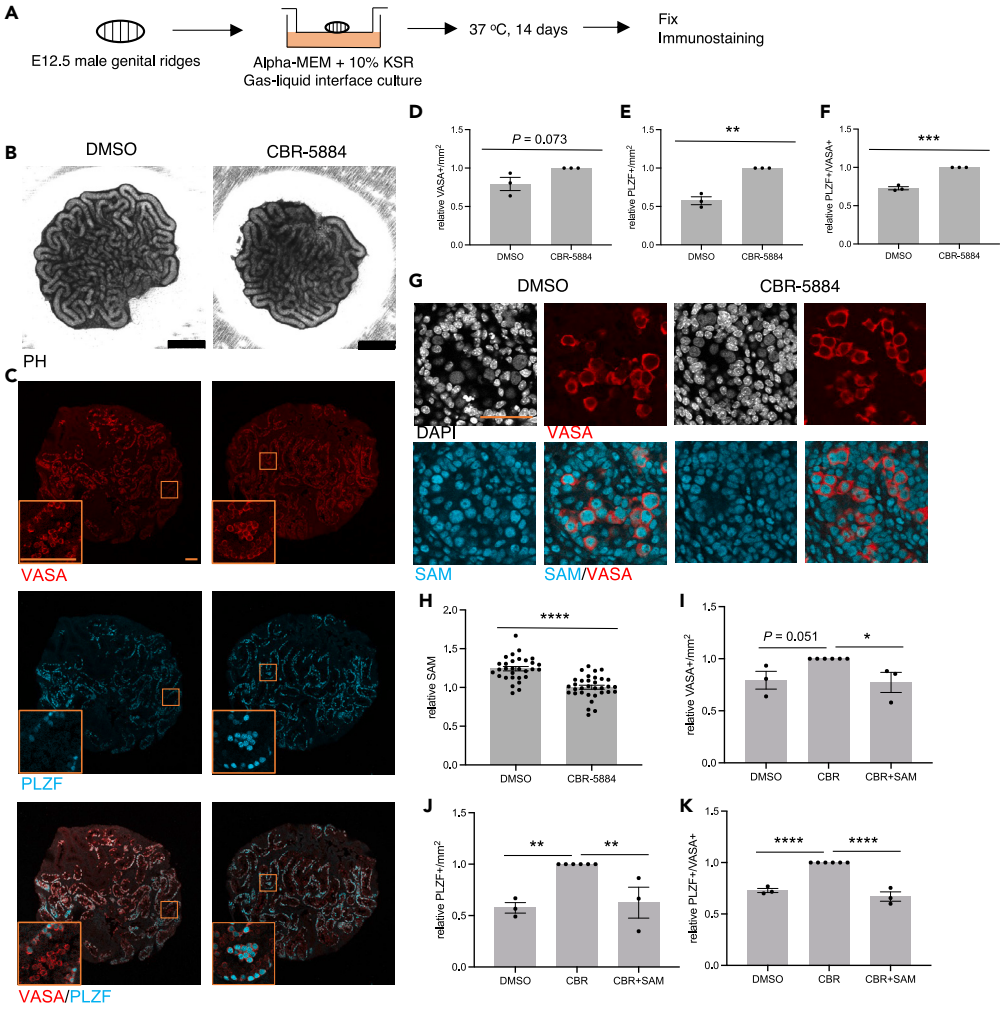

Figure 2. Effects of PHGDH inhibition in fetal testicular organ culture

(A) Schematic illustration of the fetal testes organ culture experiment.

(B) Phase-contrast microscopic image of the testes on day 14 of organ culture.

(C) Immunostaining of VASA and PLZF in testes on day 14 of organ culture. Rectangular areas correspond to enlarged images in the insets.

(D–F) Changes in the number of VASA-positive cells (D), number of PLZF-positive cells (E), and PLZF-positive rate calculated by dividing the number of PLZF-positive cells by the number of VASA-positive cells (F) following PHGDH inhibition in testes on day 14 of organ culture. Graphs present relative number of positive cells and PLZF-positive rate with the number in the culture with CBR set as 1 (two tiling sections for each replicate).

(G) Immunostaining analysis showing changes in SAM abundance following PHGDH inhibition in cultured testes at day 7.

(H) Quantification of relative fluorescence signal intensity of SAM in VASA-positive germ cells normalized to the surrounding somatic cells in cultured testes at day 7 (total of 30–33 cells from three biological replicates).

(I–K) Changes in the number of VASA-positive cells (I), number of PLZF-positive cells (J), and PLZF-positive rate calculated by dividing the number of PLZF-positive cells by the number of VASA-positive cells (K) following the addition of SAM in testes on day 14 of organ culture. Graphs present relative number of positive cells and PLZF-positive rate with the number in the culture with CBR set as 1 (two tiling sections for each replicate). Data information: values represent mean ± SE of three to six biological replicates. *$p < 0.05$, **$p < 0.01$, ***$p < 0.001$, ****$p < 0.0001$ (one-way ANOVA and Tukey's multiple comparisons test for I, J, and K, and unpaired Student's t test for D, E, F, and H). Scale bar: 500 μm (B), 100 μm (C), and 50 μm (G).

Refer also to Figure S2.

Impact of PHGDH inhibition on gene expression in male germ cells

To decipher the mechanism underlying the observed increase in the number of germ cells upon PHGDH inhibition, we examined the effect of PHGDH inhibition on gene expression. We isolated VASA-DsRed fluorescent protein (RFP)-positive germ cells from organ-cultured testes at day 14 and conducted quantitative reverse-transcription PCR (RT-qPCR) analysis of the expression of several marker genes (Figure 3A). These analyses revealed an elevation in the expression of fetal male germ cell markers (*Dnmt3l* and *Nanos2*) and stemness-related genes (*Oct4*, *Zbtb16/Plzf*, and *Id4*) in germ cells subjected to PHGDH inhibition during organ culture (Figure 3B). Acknowledging the essential roles of

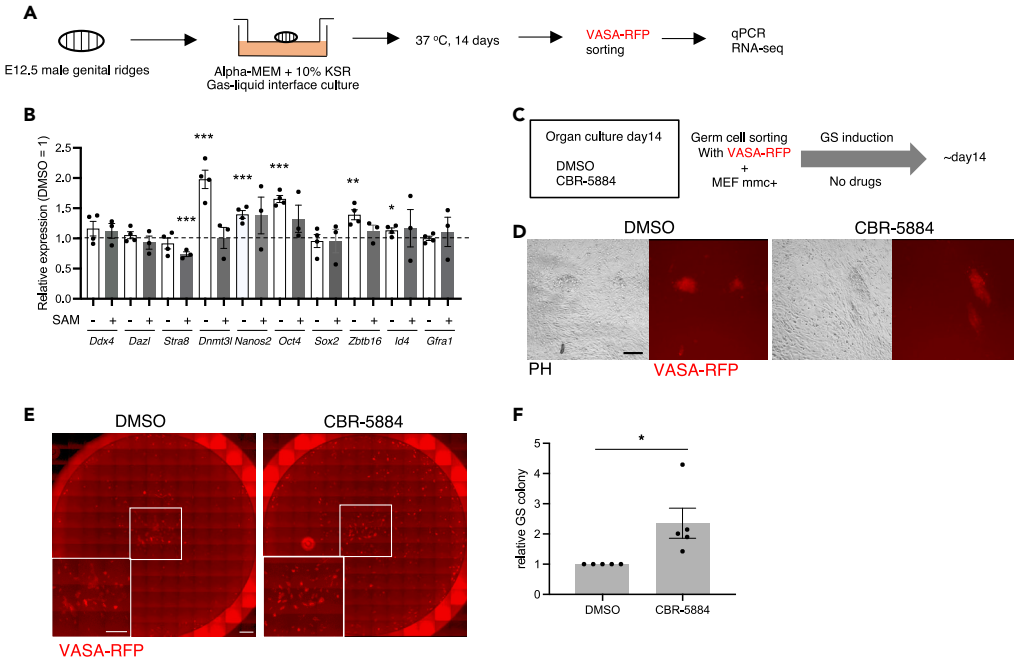

Figure 3. Impact of PHGDH inhibition on gene expression in male germ cells

(A) Schematic representation of the gene expression analysis in germ cells derived from cultured testes.

(B) RT-qPCR analysis of gene expression in germ cells isolated from cultured testes. Relative gene expression levels in germ cells treated by the PHGDH inhibitor CBR-5884 with or without SAM supplementation compared to those treated with DMSO are presented.

(C) Illustration outlining the induction of germline stem (GS) cells from cultured testes.

(D) GS cell colonies derived from VASA-RFP-positive germ cells in cultured testes at day 14.

(E) Visualization of GS cell colonies through VASA-RFP fluorescence. Colonies were observed across the wells using tiling analysis, with rectangular areas corresponding to enlarged images in the insets.

(F) Quantification of the relative number of GS colonies per well. The number of colonies from germ cells treated with DMSO was normalized to 1. Data information: values represent the mean ± SE of three to four (B) and five (E) biological replicates. Statistical significance is denoted by $*p < 0.05$, $**p < 0.01$, $***p < 0.001$ (unpaired Student's t test). Scale bar: 200 μm (D) and 1 mm (E).

Refer also to Figure S3, Tables S1, and S2 for additional details.

Oct4, *Zbtb16/Plzf*, and *Id4* in the maintenance of stemness in spermatogonial cells, as reported in previous studies,[18,19] these results suggest that inhibition of PHGDH leads to the upregulation of stemness-related genes in spermatogonia and/or an increase in the number of these cells. On the other hand, SAM supplementation partially abolished the upregulation of genes including *Dnmt3l*, *Oct4*, *and Zbtb16/Plzf* by CBR addition, indicating that the expression of at least some genes is regulated through SAM synthesized via the SGOC pathway.

To investigate whether these changes in gene expression impact the stemness of male germ cells, we attempted to induce germline stem (GS) cells[20] using sorted VASA-RFP-positive cells from cultured fetal testes in the presence of the inhibitor at day 14 (Figure 3C). In GS cell induction, based on an equivalent number of initially seeded VASA-RFP-positive cells, the PHGDH-inhibited group exhibited a significantly increased number of colonies consisting of compact clusters of cells with unclear borders (Figure 3D) characteristic of GS cells, compared with the control group (Figures 3E and 3F). These results suggest that PHGDH and SGOC metabolism plays a positive role in regulating the stemness of male germ cells.

RNA-seq analysis of PHGDH-inhibited germ cells

To gain further insights into the function of PHGDH, we conducted an RNA sequencing (RNA-seq) analysis using VASA-RFP-positive germ cells from organ-cultured testes at day 14. The marker genes whose expression changes were confirmed by qPCR showed changes in the same direction (Figure S3A). We further extracted differentially expressed genes (DEGs) through MA (log ratio versus mean average) plot analysis (Figure S3B). Subsequent functional annotation of the DEGs was carried out to discern the characteristics of these genes (Figures S3C and S3D). The group of genes downregulated by PHGDH inhibition included several stress response gene groups, such as heat shock protein genes (Figure S3C; Table S1). By contrast, the group of genes for which expression was upregulated by PHGDH inhibition encompassed many mitochondrial genes encoding proteins involved in the electron transport chain (Figure S3D; Table S2). Given the close association of these genes with cell survival, it is plausible that PHGDH and SGOC metabolism contributes not only to stemness but also to cell survival, consequently leading to an increase in the number of germ cells in cultured testes (Figure 2D).

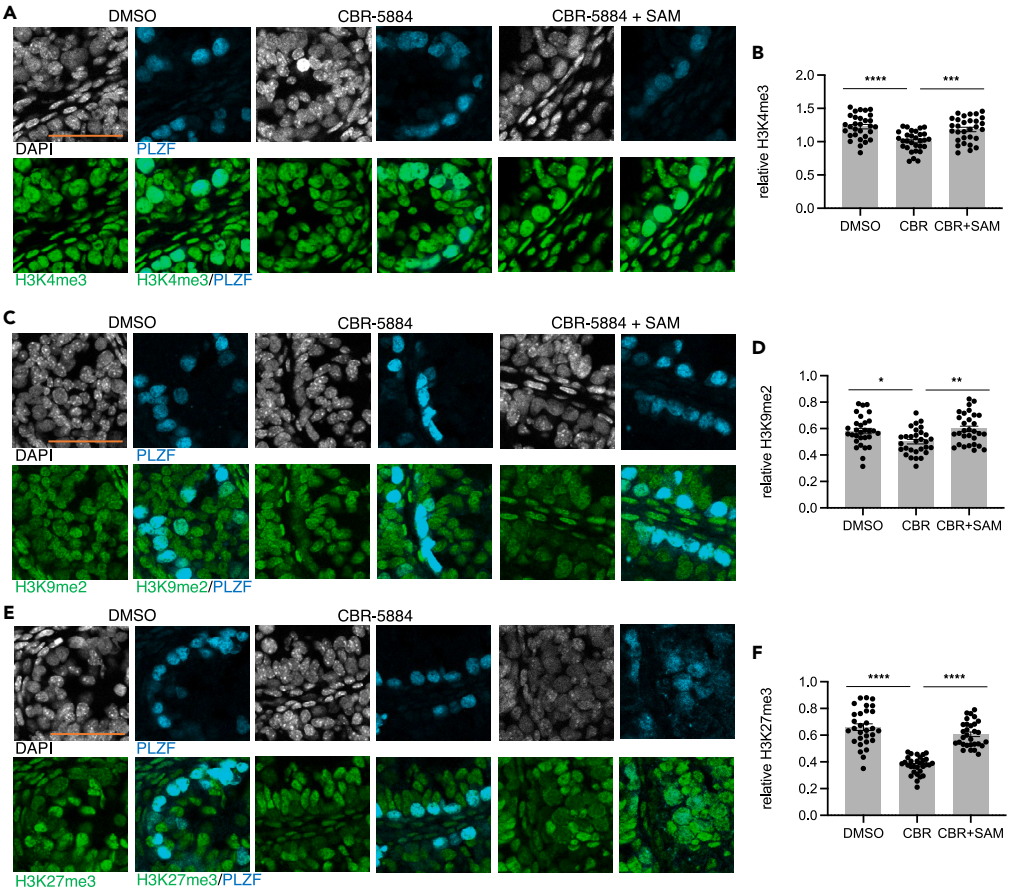

Figure 4. Effects of PHGDH inhibition on epigenomic regulation

(A, C, and E) Immunostaining analysis illustrating changes in H3K4me3 (A), H3K9me2 (C), and H3K27me3 (E) due to PHGDH inhibition with or without SAM supplementation in cultured testes at day 14.

(B, D, and F) Quantification of relative fluorescence signal intensities of H3K4me3 (B), H3K9me2 (D), and H3K27me3 (F) in PLZF-positive spermatogonial cells, normalized with surrounding somatic cells in cultured testes at day 14 (total of 30 cells from three biological replicates). Data information: values represent the mean ± SE of three biological replicates. Statistical significance is denoted by *$p < 0.05$, **$p < 0.01$, ***$p < 0.001$, ****$p < 0.0001$ (one-way ANOVA and Tukey's multiple comparisons test). Scale bar: 50 μm.

Refer also to Figure S4.

To investigate the effect of PHGDH inhibition on germ cell proliferation and survival, we assessed germ cells in the proliferative phase on day 7 of organ culture using an anti-Ki67 antibody. Interestingly, few Ki67-positive germ cells were detected, even under conditions of PHGDH inhibition (Figure S3E). Conversely, when the rate of cell death was examined using an anti-active caspase-3 antibody, a notable reduction in apoptosis of germ cells was observed under PHGDH inhibition (Figures S3F and S3G). These findings suggest that PHGDH and SGOC metabolism regulates not only male germline stemness but also cell survival.

Effect of PHGDH inhibition on epigenomic regulation

Inhibition of PHGDH is associated with a decrease in SAM synthesis, suggesting an impact on the epigenomic state of the male germ line. Therefore, we examined changes in the epigenomic state in germ cells of cultured fetal testes, focusing on histone and DNA methylation (Figures 4, S4, and S5). Concerning histone methylation, changes in histone H3 lysine 4 trimethylation (H3K4me3), H3K9 dimethylation (me2), and H3K27me3 were observed upon PHGDH inhibition. Notably, levels of H3K4me3 and H3K27me3 were significantly reduced, whereas H3K9me2 exhibited a slight decrease upon PHGDH inhibition (Figures 4B, 4D, and 4F). Notably, the histone methylation changes induced by CBR addition were significantly mitigated by SAM supplementation. Additionally, DNA methylation (5-methylcytosine, 5mC) declined significantly following PHGDH inhibition (Figures S4A and S4B). Given the enrichment of H3K4me3 in the promoter regions of key genes exhibiting reduced expression due to PHGDH inhibition in RNA-seq analysis (*heat shock protein [Hspa] 1a* and *1b* as representatives, Figure S3B), it is plausible that the observed changes in gene expression were linked to reduced H3K4me3 due to PHGDH inhibition

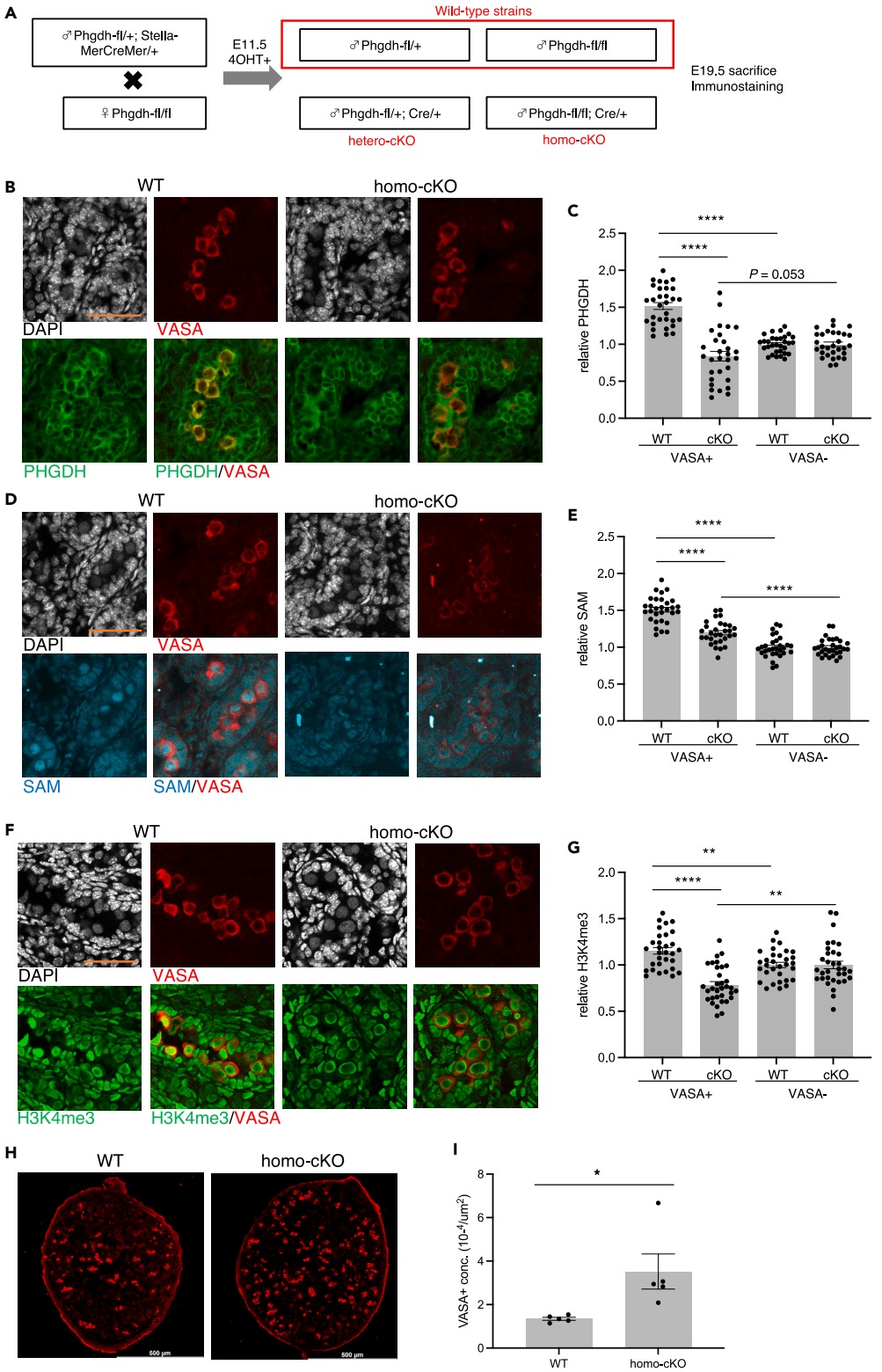

Figure 5. Male perinatal germ cell properties in *Phgdh*-cKO mice

(A) Schematic depiction of the generation of P*hgdh*-cKO mice.

(B, D, and F) Immunostaining analysis illustrating changes in PHGDH (B), SAM (D), and H3K4me3 (F) due to *Phgdh* KO in testes at E19.5.

Figure 5. *Continued*

(C, E, and G) Quantification of relative fluorescence signal intensities of PHGDH (B), SAM (D), and H3K4me3 (F) in VASA-positive germ cells normalized with surrounding somatic cells at E19.5 (total of 30–33 cells from three biological replicates).

(H) Detection of VASA-positive germ cells throughout the testicular section by tiling analysis at E19.5.

(I) Quantification of the number of VASA-positive germ cells per unit area in *Phgdh* wild-type and homo-cKO testes at E19.5 (five sections for each replicate). Data information: values represent the mean ± SE of three (C, E, G) and five (I) biological replicates. Statistical significance is indicated by N.S. (not significant), $*p < 0.05$, $***p < 0.001$, $****p < 0.0001$ (one-way ANOVA and Tukey's multiple comparisons test for C, E, G, and unpaired Student's t test for I). Scale bar: 500 μm (I), 50 μm (C, E, and G).

Refer also to Figure S5.

(Figure S4C). These observations suggest that PHGDH and SGOC metabolism plays a role in shaping the epigenome of male fetal germ cells by affecting SAM synthesis.

Perinatal germ cell differentiation in *Phgdh*-cKO mice

To genetically assess the impact of SGOC metabolism on male germ cell differentiation *in vivo*, we examined fetal male germ cells in *Phgdh*-KO mice. As PHGDH is vital for embryonic development, complete *Phgdh*-KO results in embryonic lethality around E13.5.[21] To circumvent this effect, we utilized conditional knockout (cKO) mice harboring "floxed" *Phgdh* (flanked by *loxP* sites)[22] and a *Stella-MerCreMer* transgene. The latter activates Cre recombinase production in germ cells around E11.5, with nuclear translocation occurring upon the addition of 4-hydroxytamoxifen (4OHT) (Figure 5A).[23]

We examined *Phgdh*-cKO testes at E19.5 to evaluate the effect of *Phgdh*-KO on germ cells. In homozygous *Phgdh*-cKO testes, PHGDH expression was significantly reduced, specifically in VASA-positive germ cells compared to surrounding somatic cells (Figures 5B and 5C). A decrease in the intensity of SAM (Figures 5D and 5E) and H3K4me3 (Figures 5F and 5G) was also noted in germ cells in E19.5 *Phgdh*-cKO testes, consistent with the results of PHGDH inhibition in cultured testes (Figures 2G and 4A). *Phgdh* KO also led to a slight reduction in the H3K9me2 level but had no effect on the H3K27me3 level in germ cells, results which were inconsistent with those observed in cultured testes with PHGDH inhibition (Figures S5A–S5D and 4). This inconsistency is presumably due to the difference in the stage of germ cell differentiation between the *in vitro* (E12.5 testis culture at day 14) and *in vivo* (E19.5) conditions, or the PHGDH inhibitory effects of CBR-5884 on both germ cells and somatic cells, unlike the germ cell-specific *Phgdh*-cKO. The number of VASA-positive germ cells was higher in *Phgdh* homo-cKO testes than wild-type testes, resembling the effects of PHGDH inhibition in cultured testes (Figures 5H and 5I).

Unlike testes, *Phgdh*-cKO ovaries did not exhibit distinct morphological changes, consistent with observations from cultured ovaries with PHGDH inhibition (Figure S6A). This may be due to the fact that PHGDH is barely expressed in germ cells within fetal ovaries and is only expressed in oocytes within primordial follicles, rather than in oocytes in cysts, in perinatal ovaries (Figure S6B). Therefore, we examined the changes in PHGDH expression in oocytes within primordial follicles and found a marked decrease in PHGDH expression in *Phgdh*-cKO ovaries compared with those in wild-type ovaries (Figures S6C and S6D). Correspondingly, we also observed a reduced SAM signal in *Phgdh*-cKO oocytes within primordial follicles (Figures S6E and S6F). However, *Phgdh*-cKO-dependent reduction of H3K4me3 observed in perinatal testes was not detected in oocytes within primordial follicles in neonatal ovaries (Figures S6G and S6H). These results suggest that PHGDH is strongly expressed in oocytes within primordial follicles, though its expression does not contribute to oogenesis and the maintenance of H3K4me3, at least within the ovaries at this stage.

In vitro inhibition of PHGDH was found to suppress apoptosis, potentially contributing to the increase in the number of germ cells in cultured testes (Figures S3E and S3F). To investigate whether a similar phenomenon occurred in the neonatal testes of *Phgdh*-cKO mice, we examined the apoptosis ratio in VASA-positive germ cells (Figures 6A and 6B). In wild-type testes, apoptosis of germ cells in the seminiferous tubule lumen was evident. Conversely, in *Phgdh*-cKO testes, a significant reduction in the frequency of germ cell apoptosis was noted. These findings suggest the PHGDH and SGOC pathways play a regulatory role in controlling the number of germ cells by promoting their apoptosis during the fetal and neonatal stages.

Spermatogonial transition in *Phgdh*-cKO mice

In the subsequent analysis, we examined the status of spermatogonial cells in the neonatal testes of *Phgdh*-cKO mice. *In vitro* inhibition of PHGDH resulted in an increase in the proportion of undifferentiated spermatogonial cells (Figure 2F). Similarly, we detected undifferentiated spermatogonial cells in neonatal *Phgdh*-cKO testes using PLZF immunostaining (Figure 6C). The results showed that *Phgdh*-cKO markedly increased both the number of PLZF-positive undifferentiated spermatogonia and their ratio among VASA-positive germ cells compared with those in wild-type testes (Figures 6D and 6E). The differentiation of spermatogonia in neonatal testes was also evaluated using immunostaining with anti-Sal-like protein 4 (SALL4, a spermatogonia marker)[24] and anti-cluster of differentiation 117 (CD117)/c-KIT (a marker of differentiating spermatogonia)[25] antibodies (Figures 6C–6E). The staining revealed a notable reduction in the number of c-KIT-positive differentiating cells as well as their ratios within the population of SALL4-positive spermatogonia observed in *Phgdh*-cKO testes compared to wild-type testes, whereas the number of SALL4-positive cells was not changed (Figure 6E). Taken together, the number of c-KIT-positive differentiating spermatogonia decreased, whereas the number of PLZF-positive undifferentiated spermatogonia relatively increased, though the total number of SALL4-positive spermatogonia remained unchanged. These findings suggest that PHGDH inhibition or deficiency disturbs the delicate balance between undifferentiated and differentiating spermatogonia, leading to an increase in undifferentiated spermatogonia.

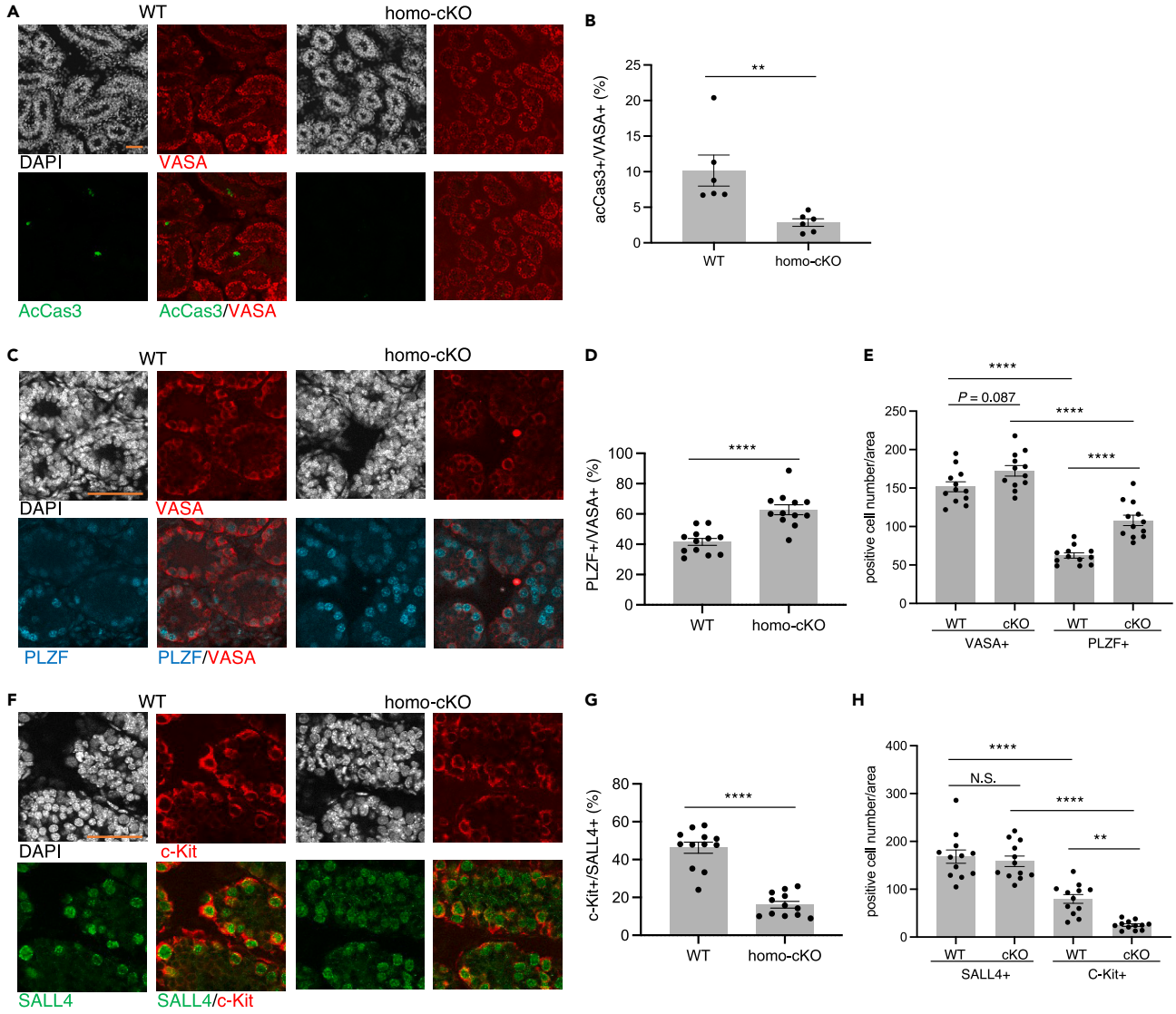

Figure 6. Spermatogonial transition in *Phgdh*-cKO mice

(A, C, and F) Immunostaining analysis illustrating changes in apoptosis (A), undifferentiated spermatogonia (C), and spermatogonial differentiation (F) due to *Phgdh* KO in testes at P7.

(B, D, and G) Quantification of the ratio of germ cells exhibiting a positive signal for active caspase-3 in VASA-positive germ cells (B), for PLZF within VASA-positive germ cells (D), or for c-KIT within SALL4-positive spermatogonia (G) in testes at P7 (two sections, four areas for each replicate).

(E and H) Quantification of germ cells exhibiting a positive signal for PLZF and/or VASA (E) or for SALL4 and/or c-KIT (H) per unit area in wild-type or *Phgdh*-KO testes at P7 (two sections, four areas for each replicate). Data information: values represent the mean ± SE of three biological replicates. Statistical significance is indicated by N.S. (not significant), $^{**}p < 0.01$, $^{****}p < 0.0001$ (one-way ANOVA and Tukey's multiple comparisons test for E and H, and unpaired Student's t test for B, D, and G). Scale bar: 50 μm.

Refer also to Figure S6.

DISCUSSION

Our investigation revealed a substantial elevation in the levels of two key components in SGOC metabolism, namely PHGDH and SAM, during the developmental stages of fetal male germ cells in mice. Additionally, we demonstrated that inhibiting PHGDH in fetal germ cells within the testes enhanced germ cell survival and increased the population of undifferentiated spermatogonia, concurrently affecting epigenomic and transcriptomic profiles. The results of this study did not, however, provide clarity as to whether the heightened undifferentiated nature of spermatogonia results from increased transition from gonocytes, inhibition of differentiation into c-KIT-positive spermatogonia, enhanced survival specific to undifferentiated spermatogonia, or suppressed survival of differentiated spermatogonia. As such, further investigation is required to address these issues and gain a more comprehensive understanding of the underlying mechanisms.

Although details regarding the mechanism underlying the specific upregulation of PHGDH in male germ cells remain elusive, previous investigations determined that expression of the *Phgdh* gene in E13.5 gonads is notably higher in male germ cells compared to somatic cells and female germ cells, indicating that PHGDH expression is regulated at the genetic level.[9,26] Several transcription factors known to induce the expression of SGOC metabolic enzyme genes have been reported.[27] In cancer cells, the genes encoding enzymes in SGOC metabolism, including *Phgdh*, are upregulated during amino acid deprivation via the general control nonderepressible 2-activating transcription factor 4 (GCN2-ATF4) signaling pathway.[28] The transcription factors NF-E2-related factor 2[29] and MYC[30] also activate SGOC metabolism, whereas hypoxia-inducible factors induce *Phgdh* gene expression under hypoxia in breast cancer cells.[31,32] N-MYC is particularly noteworthy among these factors,[33] exhibiting distinct expression patterns in male germ cells during the fetal developmental phase compared to surrounding somatic cells and female germ cells at the same stage, as previously reported.[26] These data align with the male-specific upregulation of PHGDH demonstrated in this study (Figure 1). A forthcoming challenge involves ascertaining the potential contribution of N-MYC to the transcriptional regulation of SGOC enzyme genes in the male germ line.

Apart from the regulation of *Phgdh* gene expression, regulation at the protein level has also been implicated in the augmentation of SAM synthesis. Notably, studies in colorectal cancer cells reported the monoubiquitylation of PHGDH via a cullin 4A-based E3 ligase complex, leading to enhanced catalytic activity through formation of a tetrameric structure. This process results in increased levels of serine, glycine, and SAM.[34] Consistent with this understanding, it is plausible that SAM synthesis in male germ cells is regulated not solely through PHGDH expression but also through potential modifications and/or the formation of multimers.

Interestingly, the amplification of SAM synthesis in male germ cells was predominantly observed within the nucleus, despite the upregulation of PHGDH expression occurring in the cytoplasm (Figures 1B and 1E). The specific mechanism responsible for the pronounced nuclear localization of SAM remains undetermined; however, plausible explanations include the potential nuclear localization of metabolic enzymes required for SAM synthesis downstream of PHGDH. Certainly, methionine adenosyltransferase 2A, which converts methionine to SAM, functions in both the nucleus and cytoplasm, generating nuclear SAM through interaction with the MafK oncoprotein.[35,36] The role of SAM in the nucleus primarily centers on the regulation of DNA and histone methylation, as previously reported.[37] Previous studies also reported a correlation between diminished SAM synthesis and reduced H3K4me2/3 levels across various cell types,[38–40] a finding consistent with our data illustrating a decrease in the H3K4me3 level in germ cells following PHGDH inhibition.

Furthermore, SAM exhibits anti-proliferative effects in diverse types of cancer cells, which can be attributed to its promotion of DNA methylation and concurrent downregulation of proto-oncogene expression.[41] Notably, SAM consistently induces an elevation in p53 and p21 (cell-cycle inhibitors) levels and a notable increase in the pro-apoptotic Bcl2-associated X (Bax)/B cell lymphoma 2 (Bcl2) ratio, accompanied by induction of apoptosis.[42,43] The regulatory effects observed in cancer cells as related to SAM align with the phenotypes identified in male germ cells, particularly with regard to the reduction in 5mC, increase in the number of germ cells, and diminishment of apoptosis following PHGDH inhibition. In both contexts, the modulation of SAM levels appears to affect key cellular processes, and it is therefore crucial to elucidate the mechanism by which these factors are regulated by SAM in male germ cells. This parallelism may underscore the significance of SAM and its associated metabolic pathways in governing cellular behavior and highlight the potential shared regulatory mechanisms in distinct cell types, including cancer cells and germ cells.

The current findings demonstrate an increase in the number of male fetal germ cells, which is primarily attributed to suppression of germ cell apoptosis. The transition of male germ cells to spermatogonial cells involves migration from the seminiferous tubule lumen to the basal lamina. Previous studies suggested that cells persisting in the lumen due to unsuccessful migration undergo apoptosis and subsequent elimination, potentially to remove erroneously differentiated germ cells.[4] Additionally, KO of *Bax* (pro-apoptotic) or overexpression of *Bcl2* (anti-apoptotic), thereby preventing spermatogonia apoptosis, has been shown to result in a transient augmentation of spermatogonial cells and subsequent disruption of spermatogenesis.[44,45] The impact of PHGDH inhibition on these mechanisms remains unclear at present and will therefore be a focus for future research. Additionally, investigating the impact of L-serine- and/or L-methionine-depleting dietary interventions in maternal mice on the epigenome of male fetal germ cells and their subsequent differentiation is also of significant interest.

Limitations of the study

In this article, we have outlined the roles of the SGOC pathway, encompassing PHGDH and SAM, in shaping epigenetic patterns, gene expression profiles, and cellular viability and differentiation within the male embryonic germ line in mice. However, the intricate interplay among these components remains only partially understood, necessitating further inquiry into the mechanisms underlying epigenetic dysregulation and its impact on cellular properties. Additionally, the long-term phenotypic ramifications of PHGDH-deficient germ cells in adult mice and any potential alterations in their reproductive functions have not been explored in this study. Furthermore, it is crucial to determine whether the phenotype observed in PHGDH-deficient germ cells aligns with that of naturally inactivated SGOC pathway, such as through dietary intervention utilizing a serine-deficient diet.

STAR★METHODS

Detailed methods are provided in the online version of this paper and include the following:

- KEY RESOURCES TABLE
- RESOURCE AVAILABILITY
  - Lead contact

SUPPLEMENTAL INFORMATION

Supplemental information can be found online at https://doi.org/10.1016/j.isci.2024.110702.

ACKNOWLEDGMENTS

We thank Dr. Mitinori Saitou for Dppa3-MerCreMer mice. The authors thank all members of the Cell Resource Center for Biomedical Research for helpful discussions and the Tohoku University Center of Research Instruments of the Institute of Development, Aging, and Cancer (IDAC) for use of instruments and technical support. During a portion of this work, Y.H. was supported by Grants-in-Aid for Scientific Research (KAKENHI) (grant 22K06245), KAKENHI in the Innovative Areas, "Sex Spectrum" (grant 20H04917), "Ensuring integrity in gametogenesis" (grant 19H05238), "Program of totipotency" (grant 22H04662), and a Grant-in-Aid for Transformative Research Areas (A) (grant 23H04950) from the Ministry of Education, Culture, Sports, Science and Technology of Japan (MEXT); further support was provided by the Takeda Science Foundation, Kato Memorial Bioscience Foundation, Mishima Kaiun Memorial Foundation, the Inamori Foundation, and Astellas Foundation for Research on Metabolic Disorders. Y.M. was supported by KAKENHI (grant 19H03231) from MEXT and by the Uehara Memorial Foundation.

AUTHOR CONTRIBUTIONS

Conceptualization, Y.H. and Y.M.; methodology, Y.H., Y.I.-M., A.T., and S.F.; investigation; Y.H., J.K., M.F., and K.S.; visualization, Y.H.; validation, Y.M.; writing – original draft; Y.H. and Y.M.; writing – review and editing, Y.H. and Y.M.; funding acquisition, Y.H. and Y.M.; resources, S.F.; supervision, Y.H., S.M., and Y.M.; project administration; Y.H. and Y.M.

DECLARATION OF INTERESTS

The authors declare no competing interests.

DECLARATION OF GENERATIVE AI AND AI-ASSISTED TECHNOLOGIES IN THE WRITING PROCESS

During the preparation of this work the authors used ChatGPT3.5 in order to improve academic writing in English. After using this tool, the authors reviewed and edited the content as needed and take full responsibility for the content of the publication.

Received: April 8, 2024
Revised: July 2, 2024
Accepted: August 6, 2024
Published: August 9, 2024

REFERENCES

1. Saitou, M., and Yamaji, M. (2012). Primordial germ cells in mice. Cold Spring Harb. Perspect. Biol. *4*, a008375. https://doi.org/10.1101/cshperspect.a008375.
2. Seisenberger, S., Andrews, S., Krueger, F., Arand, J., Walter, J., Santos, F., Popp, C., Thienpont, B., Dean, W., and Reik, W. (2012). The dynamics of genome-wide DNA methylation reprogramming in mouse primordial germ cells. Mol. Cell *48*, 849–862. https://doi.org/10.1016/j.molcel.2012.11.001.
3. Bowles, J., and Koopman, P. (2010). Sex determination in mammalian germ cells: extrinsic versus intrinsic factors. Reproduction *139*, 943–958. https://doi.org/10.1530/REP-10-0075.
4. Bejarano, I., Rodríguez, A.B., and Pariente, J.A. (2018). Apoptosis is a demanding selective tool during the development of fetal male germ cells. Front. Cell Dev. Biol. *6*, 65. https://doi.org/10.3389/fcell.2018.00065.
5. Western, P.S., Miles, D.C., van den Bergen, J.A., Burton, M., and Sinclair, A.H. (2008). Dynamic regulation of mitotic arrest in fetal male germ cells. Stem Cell. *26*, 339–347. https://doi.org/10.1634/stemcells.2007-0622.
6. Spradling, A., Fuller, M.T., Braun, R.E., and Yoshida, S. (2011). Germline stem cells. Cold Spring Harb. Perspect. Biol. *3*, a002642. https://doi.org/10.1101/cshperspect.a002642.
7. Lei, L., and Spradling, A.C. (2013). Mouse primordial germ cells produce cysts that partially fragment prior to meiosis. Development *140*, 2075–2081. https://doi.org/10.1242/dev.093864.
8. Hayashi, Y., Otsuka, K., Ebina, M., Igarashi, K., Takehara, A., Matsumoto, M., Kanai, A., Igarashi, K., Soga, T., and Matsui, Y. (2017). Distinct requirements for energy metabolism

in mouse primordial germ cells and their reprogramming to embryonic germ cells. Proc. Natl. Acad. Sci. USA *114*, 8289–8294. https://doi.org/10.1073/pnas.1620915114.

9. Hayashi, Y., Mori, M., Igarashi, K., Tanaka, K., Takehara, A., Ito-Matsuoka, Y., Kanai, A., Yaegashi, N., Soga, T., and Matsui, Y. (2020). Proteomic and metabolomic analyses uncover sex-specific regulatory pathways in mouse fetal germline differentiation. Biol. Reprod. *103*, 717–735. https://doi.org/10.1093/biolre/ioaa115.
10. Teng, H., Sui, X., Zhou, C., Shen, C., Yang, Y., Zhang, P., Guo, X., and Huo, R. (2016). Fatty acid degradation plays an essential role in proliferation of mouse female primordial germ cells via the p53-dependent cell cycle regulation. Cell Cycle *15*, 425–431. https://doi.org/10.1080/15384101.2015.1127473.
11. Tanaka, K., Hayashi, Y., Takehara, A., Ito-Matsuoka, Y., Tachibana, M., Yaegashi, N., and Matsui, Y. (2021). Abnormal early folliculogenesis due to impeded pyruvate metabolism in mouse oocytes. Biol. Reprod. *105*, 64–75. https://doi.org/10.1093/biolre/ioab064.
12. Hayashi, Y., and Matsui, Y. (2022). Metabolic control of germline formation and differentiation in mammal. Sex. Dev. *16*, 388–403. https://doi.org/10.1159/000520662.
13. Matsui, Y., and Hayashi, Y. (2022). Metabolic pathways regulating the development and non-genomic heritable traits of germ cells. J. Reprod. Dev. *68*, 96–103. https://doi.org/10.1262/jrd.2021-137.
14. Sabari, B.R., Zhang, D., Allis, C.D., and Zhao, Y. (2017). Metabolic regulation of gene expression through histone acylations. Nat. Rev. Mol. Cell Biol. *18*, 90–101. https://doi.org/10.1038/nrm.2016.140.
15. Haws, S.A., Leech, C.M., and Denu, J.M. (2020). Metabolism and the epigenome: A dynamic relationship. Trends Biochem. Sci. *45*, 731–747. https://doi.org/10.1016/j.tibs.2020.04.002.
16. Ishikura, Y., Yabuta, Y., Ohta, H., Hayashi, K., Nakamura, T., Okamoto, I., Yamamoto, T., Kurimoto, K., Shirane, K., Sasaki, H., and Saitou, M. (2016). In vitro derivation and propagation of spermatogonial stem cell activity from mouse pluripotent stem cells. Cell Rep. *17*, 2789–2804. https://doi.org/10.1016/j.celrep.2016.11.026.
17. Chaneton, B., Hillmann, P., Zheng, L., Martin, A.C.L., Maddocks, O.D.K., Chokkathukalam, A., Coyle, J.E., Jankevics, A., Holding, F.P., Vousden, K.H., et al. (2012). Serine is a natural ligand and allosteric activator of pyruvate kinase M2. Nature *491*, 458–462. https://doi.org/10.1038/nature11540.
18. Dann, C.T., Alvarado, A.L., Molyneux, L.A., Denard, B.S., Garbers, D.L., and Porteus, M.H. (2008). Spermatogonial stem cell self-renewal requires OCT4, a factor downregulated during retinoic acid-induced differentiation. Stem Cell. *26*, 2928–2937. https://doi.org/10.1634/stemcells.2008-0134.
19. Oatley, M.J., Kaucher, A.V., Racicot, K.E., and Oatley, J.M. (2011). Inhibitor of DNA binding 4 is expressed selectively by single spermatogonia in the male germline and regulates the self-renewal of spermatogonial stem cells in mice. Biol. Reprod. *85*, 347–356. https://doi.org/10.1095/biolreprod.111.091330.
20. Kanatsu-Shinohara, M., Ogonuki, N., Inoue, K., Miki, H., Ogura, A., Toyokuni, S., and Shinohara, T. (2003). Long-term proliferation in culture and germline transmission of mouse male germline stem cells. Biol. Reprod. *69*, 612–616. https://doi.org/10.1095/biolreprod.103.017012.
21. Yoshida, K., Furuya, S., Osuka, S., Mitoma, J., Shinoda, Y., Watanabe, M., Azuma, N., Tanaka, H., Hashikawa, T., Itohara, S., and Hirabayashi, Y. (2004). Targeted disruption of the mouse 3-phosphoglycerate dehydrogenase gene causes severe neurodevelopmental defects and results in embryonic lethality. J. Biol. Chem. *279*, 3573–3577. https://doi.org/10.1074/jbc.C300507200.
22. Yang, J.H., Wada, A., Yoshida, K., Miyoshi, Y., Sayano, T., Esaki, K., Kinoshita, M.O., Tomonaga, S., Azuma, N., Watanabe, M., et al. (2010). Brain-specific Phgdh deletion reveals a pivotal role for L-serine biosynthesis in controlling the level of D-serine, an N-methyl-D-aspartate receptor co-agonist, in adult brain. J. Biol. Chem. *285*, 41380–41390. https://doi.org/10.1074/jbc.M110.187443.
23. Hirota, T., Ohta, H., Shigeta, M., Niwa, H., and Saitou, M. (2011). Drug-inducible gene recombination by the Dppa3-MER Cre MER transgene in the developmental cycle of the germ cell lineage in mice. Biol. Reprod. *85*, 367–377. https://doi.org/10.1095/biolreprod.110.090662.
24. Gassei, K., and Orwig, K.E. (2013). SALL4 expression in gonocytes and spermatogonial clones of postnatal mouse testes. PLoS One *8*, e53976. https://doi.org/10.1371/journal.pone.0053976.
25. Yoshida, S., Sukeno, M., Nakagawa, T., Ohbo, K., Nagamatsu, G., Suda, T., and Nabeshima, Y.i. (2006). The first round of mouse spermatogenesis is a distinctive program that lacks the self-renewing spermatogonia stage. Development *133*, 1495–1505. https://doi.org/10.1242/dev.02316.
26. Percharde, M., Wong, P., and Ramalho-Santos, M. (2017). Global hypertranscription in the mouse embryonic germline. Cell Rep. *19*, 1987–1996. https://doi.org/10.1016/j.celrep.2017.05.036.
27. Sun, W., Liu, R., Gao, X., Lin, Z., Tang, H., Cui, H., and Zhao, E. (2023). Targeting serine-glycine-one-carbon metabolism as a vulnerability in cancers. Biomark. Res. *11*, 48. https://doi.org/10.1186/s40364-023-00487-4.
28. Zhao, E., Ding, J., Xia, Y., Liu, M., Ye, B., Choi, J.H., Yan, C., Dong, Z., Huang, S., Zha, Y., et al. (2016). KDM4C and ATF4 cooperate in transcriptional control of amino acid metabolism. Cell Rep. *14*, 506–519. https://doi.org/10.1016/j.celrep.2015.12.053.
29. DeNicola, G.M., Chen, P.H., Mullarky, E., Sudderth, J.A., Hu, Z., Wu, D., Tang, H., Xie, Y., Asara, J.M., Huffman, K.E., et al. (2015). NRF2 regulates serine biosynthesis in non-small cell lung cancer. Nat. Genet. *47*, 1475–1481. https://doi.org/10.1038/ng.3421.
30. Nilsson, L.M., Forshell, T.Z.P., Rimpi, S., Kreutzer, C., Pretsch, W., Bornkamm, G.W., and Nilsson, J.A. (2012). Mouse genetics suggests cell-context dependency for myc-regulated metabolic enzymes during tumorigenesis. PLoS Genet. *8*, e1002573. https://doi.org/10.1371/journal.pgen.1002573.
31. Yoshino, H., Nohata, N., Miyamoto, K., Yonemori, M., Sakaguchi, T., Sugita, S., Itesako, T., Kofuji, S., Nakagawa, M., Dahiya, R., and Enokida, H. (2017). PHGDH as a key enzyme for serine biosynthesis in HIF2α-targeting therapy for renal cell carcinoma. Cancer Res. *77*, 6321–6329. https://doi.org/10.1158/0008-5472.CAN-17-1589.
32. Nagao, A., Kobayashi, M., Koyasu, S., Chow, C.C.T., and Harada, H. (2019). HIF-1-dependent reprogramming of glucose metabolic pathway of cancer cells and its therapeutic significance. Int. J. Mol. Sci. *20*, 238. https://doi.org/10.3390/ijms20020238.
33. Xia, Y., Ye, B., Ding, J., Yu, Y., Alptekin, A., Thangaraju, M., Prasad, P.D., Ding, Z.C., Park, E.J., Choi, J.H., et al. (2019). Metabolic Reprogramming by MYCN Confers Dependence on the Serine-Glycine-One-Carbon Biosynthetic Pathway. Cancer Res. *79*, 3837–3850. https://doi.org/10.1158/0008-5472.CAN-18-3541.
34. Zhang, Y., Yu, H., Zhang, J., Gao, H., Wang, S., Li, S., Wei, P., Liang, J., Yu, G., Wang, X., et al. (2021). Cul4A-DDB1-mediated monoubiquitination of phosphoglycerate dehydrogenase promotes colorectal cancer metastasis via increased S-adenosylmethionine. J. Clin. Invest. *131*, e146187. https://doi.org/10.1172/JCI146187.
35. Katoh, Y., Ikura, T., Hoshikawa, Y., Tashiro, S., Ito, T., Ohta, M., Kera, Y., Noda, T., and Igarashi, K. (2011). Methionine adenosyltransferase II serves as a transcriptional corepressor of Maf oncoprotein. Mol. Cell *41*, 554–566. https://doi.org/10.1016/j.molcel.2011.02.018.
36. Boon, R. (2021). Metabolic Fuel for Epigenetic: Nuclear Production Meets Local Consumption. Front. Genet. *12*, 768996. https://doi.org/10.3389/fgene.2021.768996.
37. He, Y., Gao, M., Tang, H., Cao, Y., Liu, S., and Tao, Y. (2019). Metabolic intermediates in tumorigenesis and progression. Int. J. Biol. Sci. *15*, 1187–1199. https://doi.org/10.7150/ijbs.33496.
38. Shyh-Chang, N., Locasale, J.W., Lyssiotis, C.A., Zheng, Y., Teo, R.Y., Ratanasirintrawoot, S., Zhang, J., Onder, T., Unternaehrer, J.J., Zhu, H., et al. (2013). Influence of threonine metabolism on S-adenosylmethionine and histone methylation. Science *339*, 222–226. https://doi.org/10.1126/science.1226603.
39. Shiraki, N., Shiraki, Y., Tsuyama, T., Obata, F., Miura, M., Nagae, G., Aburatani, H., Kume, K., Endo, F., and Kume, S. (2014). Methionine metabolism regulates maintenance and differentiation of human pluripotent stem cells. Cell Metab. *19*, 780–794. https://doi.org/10.1016/j.cmet.2014.03.017.
40. Mentch, S.J., Mehrmohamadi, M., Huang, L., Liu, X., Gupta, D., Mattocks, D., Gómez Padilla, P., Ables, G., Bamman, M.M., Thalacker-Mercer, A.E., et al. (2015). Histone methylation dynamics and gene regulation occur through the sensing of one-carbon metabolism. Cell Metab. *22*, 861–873. https://doi.org/10.1016/j.cmet.2015.08.024.
41. Schmidt, T., Leha, A., and Salinas-Riester, G. (2016). Treatment of prostate cancer cells with S-adenosylmethionine leads to genome-wide alterations in transcription profiles. Gene *595*, 161–167. https://doi.org/10.1016/j.gene.2016.09.032.
42. Ilisso, C.P., Sapio, L., Delle Cave, D., Illiano, M., Spina, A., Cacciapuoti, G., Naviglio, S., and Porcelli, M. (2016). S-Adenosylmethionine affects ERK1/2 and Stat3 pathways and induces apotosis in osteosarcoma cells. J. Cell. Physiol. *231*, 428–435. https://doi.org/10.1002/jcp.25089.
43. Stiuso, P., Bagarolo, M.L., Ilisso, C.P., Vanacore, D., Martino, E., Caraglia, M., Porcelli, M., and Cacciapuoti, G. (2016). Protective effect of tyrosol and

S-adenosylmethionine against ethanol-induced oxidative stress of Hepg2 cells involves Sirtuin 1, P53 and Erk1/2 signaling. Int. J. Mol. Sci. *17*, 622. https://doi.org/10.3390/ijms17050622.

44. Furuchi, T., Masuko, K., Nishimune, Y., Obinata, M., and Matsui, Y. (1996). Inhibition of testicular germ cell apoptosis and differentiation in mice misexpressing Bcl-2 in spermatogonia. Development *122*, 1703–1709. https://doi.org/10.1242/dev.122.6.1703.
45. Russell, L.D., Chiarini-Garcia, H., Korsmeyer, S.J., and Knudson, C.M. (2002). Bax-dependent spermatogonia apoptosis is required for testicular development and spermatogenesis. Biol. Reprod. *66*, 950–958. https://doi.org/10.1095/biolreprod66.4.950.
46. Imamura, M., Aoi, T., Tokumasu, A., Mise, N., Abe, K., Yamanaka, S., and Noce, T. (2010). Induction of primordial germ cells from mouse induced pluripotent stem cells derived from adult hepatocytes. Mol. Reprod. Dev. *77*, 802–811. https://doi.org/10.1002/mrd.21223.
47. Chen, S., Zhou, Y., Chen, Y., and Gu, J. (2018). fastp: an ultra-fast all-in-one FASTQ preprocessor. Bioinformatics *34*, i884–i890. https://doi.org/10.1093/bioinformatics/bty560.
48. Bray, N.L., Pimentel, H., Melsted, P., and Pachter, L. (2016). Near-optimal probabilistic RNA-seq quantification. Nat. Biotechnol. *34*, 525–527. https://doi.org/10.1038/nbt.3519.
49. Love, M.I., Huber, W., and Anders, S. (2014). Moderated estimation of fold change and dispersion for RNA-seq data with DESeq2. Genome Biol. *15*, 550. https://doi.org/10.1186/s13059-014-0550-8.
50. Zhou, Y., Zhou, B., Pache, L., Chang, M., Khodabakhshi, A.H., Tanaseichuk, O., Benner, C., and Chanda, S.K. (2019). Metascape provides a biologist-oriented resource for the analysis of systems-level datasets. Nat. Commun. *10*, 1523. https://doi.org/10.1038/s41467-019-09234-6.
51. Krueger, F., and Andrews, S.R. (2011). Bismark: a flexible aligner and methylation caller for Bisulfite-Seq applications. Bioinformatics *27*, 1571–1572. https://doi.org/10.1093/bioinformatics/btr167.
52. Langmead, B., and Salzberg, S.L. (2012). Fast gapped-read alignment with Bowtie 2. Nat. Methods *9*, 357–359. https://doi.org/10.1038/nmeth.1923.
53. Li, H., and Durbin, R. (2009). Fast and accurate short read alignment with Burrows–Wheeler transform. Bioinformatics *25*, 1754–1760. https://doi.org/10.1093/bioinformatics/btp324.
54. Ramírez, F., Dündar, F., Diehl, S., Grüning, B.A., and Manke, T. (2014). deepTools: a flexible platform for exploring deep-sequencing data. Nucleic Acids Res. *42*, W187–W191. https://doi.org/10.1093/nar/gku365.
55. Morohaku, K., Hirao, Y., and Obata, Y. (2017). Development of fertile mouse oocytes from mitotic germ cells in vitro. Nat. Protoc. *12*, 1817–1829. https://doi.org/10.1038/nprot.2017.069.
56. Kobayashi, H., Sakurai, T., Miura, F., Imai, M., Mochiduki, K., Yanagisawa, E., Sakashita, A., Wakai, T., Suzuki, Y., Ito, T., et al. (2013). High-resolution DNA methylome analysis of primordial germ cells identifies gender-specific reprogramming in mice. Genome Res. *23*, 616–627. https://doi.org/10.1101/gr.148023.112.
57. Kubo, N., Toh, H., Shirane, K., Shirakawa, T., Kobayashi, H., Sato, T., Sone, H., Sato, Y., Tomizawa, S.i., Tsurusaki, Y., et al. (2015). DNA methylation and gene expression dynamics during spermatogonial stem cell differentiation in the early postnatal mouse testis. BMC Genom. *16*, 624. https://doi.org/10.1186/s12864-015-1833-5.
58. Shirane, K., Miura, F., Ito, T., and Lorincz, M.C. (2020). NSD1-deposited H3K36me2 directs de novo methylation in the mouse male germline and counteracts Polycomb-associated silencing. Nat. Genet. *52*, 1088–1098. https://doi.org/10.1038/s41588-020-0689-z.
59. Nassar, L.R., Barber, G.P., Benet-Pagès, A., Casper, J., Clawson, H., Diekhans, M., Fischer, C., Gonzalez, J.N., Hinrichs, A.S., Lee, B.T., et al. (2023). The UCSC Genome Browser database: 2023 update. Nucleic Acids Res. *51*, D1188–D1195. https://doi.org/10.1093/nar/gkac1072.

STAR★METHODS

KEY RESOURCES TABLE

REAGENT or RESOURCE	SOURCE	IDENTIFIER
Antibodies		
Goat polyclonal anti-VASA	Novus Biologicals	Cat#AF2030; RRID: AB_2277369
Rabbit polyclonal anti-PHGDH	Frontier Institute	Cat#MSFR100010; RRID: AB_2571653
Mouse monoclonal anti-PLZF [D-9] (with or without Alexa 647 conjugation)	Santa Cruz	Cat#sc-28319; RRID: AB_2218941
Mouse monoclonal anti-SAM (Alexa 647-conjugated)	Arthus Biosystems	Cat#MAF00201
Rabbit polyclonal anti-H3K4me3	abcam	Cat#ab8580; RRID: AB_306649
Rabbit polyclonal anti-H3K4me3	Millipore	Cat#07–473; RRID: AB_1977252
Rabbit polyclonal anti-H3K9me2	Millipore	Cat#07–441; RRID: AB_310619
Rabbit polyclonal anti-H3K27me3	Millipore	Cat#07–449; RRID: AB_310624
Rabbit monoclonal anti-5mC [RM231]	abcam	Cat#ab214727
Rat monoclonal anti-Ki67 (SolA15)	Invitrogen	Cat#14-5698-82; RRID: AB_10854564
Rabbit monoclonal anti–active caspase-3	BD Biosciences	Cat#559565; RRID: AB_397274
Rabbit polyclonal anti-SALL4	abcam	Cat#ab29112; RRID: AB_777810
Goat polyclonal anti–c-KIT	R&D	Cat#AF1356; RRID: AB_354750
Donkey polyclonal Alexa Fluor 488 anti-rabbit IgG	Thermo Fisher Scientific	Cat#A-21206; RRID: AB_2535792
Donkey polyclonal Alexa Fluor 488 anti-rat IgG	Thermo Fisher Scientific	Cat#A-21208; RRID: AB_2535794
Donkey polyclonal Alexa Fluor 568 anti-goat IgG	Thermo Fisher Scientific	Cat#A-11057; RRID: AB_2534104
Donkey polyclonal Alexa Fluor 647 anti-mouse IgG	Thermo Fisher Scientific	Cat#A-31571; RRID: AB_162542
Chemicals, peptides, and recombinant proteins		
Leukemia inhibitory factor (LIF)	Millipore	ESG1107
CBR-5884	Cayman Chemical	19236
S-(5′-Adenosyl)-L-methionine chloride dihydrochloride	Sigma-Aldrich	A7007
SuperScript III Reverse Transcriptase	Thermo Fisher Scientific	18080044
Power SYBR Green PCR Master Mix	Applied Biosystems	4368708
EGF	R&D	2028-EG-200
bFGF	Sigma-Aldrich	F0291
GDNF, Rat, Recombinant	R&D	512-GF
4-Hydroxytamoxifen	Sigma-Aldrich	H6278
GlutaMAX-I	Gibco	35050–061
Insulin-Transferrin-Selenium (ITS -G)	Thermo Fisher Scientific	41400–045
AlbuMAX-II	Thermo Fisher Scientific	11021–029
ICI182780	R&D	1047
Critical commercial assays		
RNeasy Micro Kit	QIAGEN	74004
TruSeq RNA Library Prep Kit	Illumina	RS-122-2001
Deposited data		
RNA-seq data	This paper	GEO: GSE263499
Raw data from all figures	This paper	https://doi.org/10.17632/6kwcf49khc.1

(*Continued on next page*)

Continued

REAGENT or RESOURCE	SOURCE	IDENTIFIER
Experimental models: organisms/strains		
Mouse: B6.129P2 Vasa:RFP transgenic	RIKEN BRC	Imamura et al.[46]
Mouse: C57BL/6J Phgdh-flox	Dr. Shigeki Furuya	Yang et al.[22]
Mouse: C57BL/6J Dppa3-MerCreMer	Dr. Mitinori Saitou	Hirota et al.[23]
Oligonucleotides		
Primers for genotyping PCR of Phgdh-flox Forward: 5′-CATGAGGAACTGAACTGAAGGATTGA-3′	FASMAC	Yang et al.[22]
Primers for genotyping PCR of Phgdh-flox Reverse: 5′-CAAGGAGGCTCACACATCCCAGAAC-3′	FASMAC	Yang et al.[22]
Primers for genotyping PCR of Dppa3-MerCreMer Forward: 5′-CATACAGGCTGCATCGGTAAC-3′	FASMAC	Hirota et al.[23]
Primers for genotyping PCR of Dppa3-MerCreMer Reverse: 5′-CTTGTCATCGTCATCCTTGTAATCGATG-3′	FASMAC	Hirota et al.[23]
Primers for genotyping PCR of Dppa3-MerCreMer Internal control reverse: 5′-TCTGGTTGTAGGACGTCTGAAACAG-3′	FASMAC	Hirota et al.[23]
Primers for RT-qPCR, see Table S3	FASMAC	N/A
Software and algorithms		
fastp	Chen et al.[47]	https://github.com/OpenGene/fastp
kallisto	Bray et al.[48]	https://github.com/pachterlab/kallisto
DESeq2	Love et al.[49]	https://bioconductor.org/packages/release/bioc/html/DESeq2.html
Metascape	Zhou et al.[50]	https://metascape.org/gp/index.html#/main/step1
Venn diagram (Bioinformatics & Evolutionary Genomics)	N/A	https://bioinformatics.psb.ugent.be/webtools/Venn/
Trim Galore!	N/A	https://github.com/FelixKrueger/TrimGalore
Bismark	Krueger and Andrews[51]	https://github.com/FelixKrueger/Bismark
Bowtie2	Langmead and Salzberg[52]	https://github.com/BenLangmead/bowtie2
bwa	Li and Durbin[53]	https://github.com/lh3/bwa
Picard tools	N/A	http://broadinstitute.github.io/picard
Samtools	N/A	http://www.htslib.org/
DeepTools	Ramirez et al.[54]	https://github.com/deeptools/deepTools
Leica Application Suite X (LAS X)	Leica	RRID: SCR_013673
GraphPad Prism version 10.2.2 for MacOS	GraphPad Software	www.graphpad.com

RESOURCE AVAILABILITY

Lead contact

Further information and requests for resources and reagents should be directed to and will be fulfilled by the Lead Contact, Yasuhisa Matsui (yasuhisa.matsui.d3@tohoku.ac.jp).

Materials availability

This study did not generate new unique reagents.

Data and code availability

- All RNA-seq fastq files generated in this study have been uploaded to the Gene Expression Omnibus (GEO) under accession number GSE263499 (https://www.ncbi.nlm.nih.gov/geo/query/acc.cgi?acc=GSE263499). This paper does not report original code. Raw data from all figures were deposited on Mendeley at https://doi.org/10.17632/6kwcf49khc.1.
- Any additional information required to reanalyze the data reported in this paper is available from the lead contact upon request.

EXPERIMENTAL MODEL AND STUDY PARTICIPANT DETAILS

Mice

Multi-cross hybrid (MCH) mice were obtained from Japan SLC, Inc. The C57BL/6J *Phgdh-flox* mouse strain was detailed in the work by Yang et al. (2010).[22] Fetal germ cell–specific *Phgdh*-cKO mice were generated by crossbreeding *Phgdh-flox* mice with male *Stella-MerCreMer* mice aged 2 to 10 months,[23] and a 100-μL intraperitoneal injection of 10 mg/mL 4-OHT in corn oil was administered at E11.5. Fetal or neonatal mice were dissected at E19.5 or P7, respectively. The mice were housed and bred in the Animal Unit of the Institute of Development, Aging, and Cancer (Tohoku University), an environmentally controlled and specific-pathogen-free facility. All animal experiments conducted in this study adhered to the ethical guidelines of Tohoku University, and the corresponding protocols were thoroughly reviewed and approved by the Tohoku University Animal Studies Committee (approval number: 2019AcA-026-01).

Culture of mouse fetal testes and ovaries

Male B6C3F1 homozygous VASA-RFP mice[46] were bred with female MCH mice aged 2 to 10 months to obtain fetuses. Upon separating the testes from the fetuses at E12.5, the testes were transferred to wells with Transwell Collagen-Coated PTFE Membrane Inserts (Transwell-COL, Costar, pore size: 3 μm) in either 6-well or 12-well plates containing α-minimum essential medium (α-MEM, Invitrogen) supplemented with 10% KnockOut Serum Replacement and 1% penicillin/streptomycin (modified from Ishikura et al., 2016).[16] The cultures were maintained at 37°C with 5% CO_2 in a gas-liquid interphase setup. Each well received either 1.3 mL (for 6-well plates) or 500 μL (for 12-well plates) of medium, and the medium was refreshed weekly. For inhibition of PHGDH, 20 μM CBR-5884 was introduced to the culture medium (with 0.04% DMSO as the control). Compensation experiments were performed with the addition of 100 μM SAM or 0.4 mM L-serine to the culture medium.

Ovarian culture was performed according to methods presented in previous study.[55] E12.5 VASA-RFP ovaries were transferred to wells with Transwell-COL in 6-well plates containing 2.02 mL of α-MEM supplemented with 10% FBS, 0.5 mg/mL 2-*O*-alpha-*d*-glucopyranosyl-*l*-ascorbic acid, and 1% penicillin/streptomycin. The cultures were maintained at 37°C with 5% CO_2, and the medium was changed half of the volume every 2 days. From days 5–11, 5 μM of an estrogen receptor antagonist, ICI182780, was added to the medium.

Cell culture

Murine GS cell induction was conducted following established protocols.[16,20] Briefly, cultured testes were incubated with 0.05% Trypsin-EDTA for 15 min, with intermittent pipetting every 5 min. The enzymatic reaction was halted using DMEM with 10% FBS, and the cells were dissociated into single cells through vigorous pipetting. The cell suspension was then centrifuged at 1,000 rpm for 5 min, and the supernatant was discarded. The resulting cell pellet was resuspended in DMEM with 2% FBS and subjected to sorting based on the VASA-RFP signal using an S3e cell sorter (BIO-RAD). After centrifugation and removal of the supernatant, the cell pellet was resuspended in GS culture medium containing growth factors and plated on 0.1% (w/v) gelatin-coated culture plates with MEF feeder cells. The cultures were maintained at 37°C with 5% CO_2. Following two or three passages, remaining VASA-RFP–positive GS colonies were expanded and quantified for subsequent analysis.

The GS culture medium, as described by Ishikura et al. (2016),[16] comprised StemPro-34 SFM (Invitrogen) supplemented with StemPro supplement (Gibco), 1% FBS, 1× GlutaMAX-I (Gibco), 1× MEM vitamin solution (Gibco), 5 mg/mL AlbuMAX-II, 5×10^{-5} M 2-mercaptoethanol, 1× MEM nonessential amino acids (Gibco), 30 mg/mL sodium pyruvate (Gibco), 1× ITS-G, 100 U/mL penicillin, 0.1 mg/mL streptomycin, and growth factors (recombinant rat GDNF [10 ng/mL], human bFGF [10 ng/mL], LIF/ESGRO [10^3 U/mL], and mouse EGF [20 ng/mL]).

METHOD DETAILS

RT-qPCR analysis

Total RNA was extracted from VASA-RFP sorted germ cells and purified utilizing an rNeasy Micro Kit. Reverse transcription of total RNA was performed using Superscript III, and the resulting cDNAs were employed for quantitative PCR using Power SYBR Green PCR Master Mix. PCR signals were detected using a CFX Connect Real-Time PCR Detection System (BioRad). The sequences of the PCR primers are shown in Table S3.

RNA-seq

RNA-seq libraries were generated from two biological replicates of VASA-RFP sorted germ cells of cultured testes on day 14 after induction (0.04% DMSO group vs. 20 μM CBR-5884 group). Each library was constructed using a TruSeq RNA Library Preparation Kit, starting from 100 ng of total RNA. Subsequently, the libraries were sequenced on an Illumina HiSeq 2500 instrument, producing reads through 50-bp single-end sequencing. The generated reads were trimmed using fastp software.[47] For gene expression analysis, the reads were aligned to the mouse genome (UCSC mm10 genome assembly and NCBI RefSeq database) using kallisto software,[48] considering an estimated average fragment length of 50. This was followed by calculation of read counts and TPM (transcripts per million). Public databases were utilized, including bSgenome.Mmusculus.UCSC.mm10 (https://bioconductor.org/packages/release/data/annotation/html/bSgenome.Mmusculus.UCSC.mm10.html) and TxDb.Mmusculus.UCSC.mm10.knownGene (https://bioconductor.org/packages/release/data/annotation/html/TxDb.Mmusculus.UCSC.mm10.knownGene.html). DESeq2[49] was employed to identify differentially expressed genes (DEGs), with statistical significance determined using the Wald test. Genes exhibiting statistically significant differences ($p < 0.05$) were classified as DEGs (only genes with a mean TPM exceeding 1 were considered). Functional enrichment analysis of DEGs was conducted using Metascape.[50] Venn diagrams were calculated and visualized using the Bioinformatics & Evolutionary Genomics website.

Re-analysis of previously published whole-genome bisulfite sequencing (WGBS) or chromatin immunoprecipitation (ChIP)-seq data

WGBS data from previous studies (DRA000607, DRA002477 and DRA002402)[56,57] was reprocessed by the following methods.[58] Briefly, adaptor sequences at the 5′ end and low-quality bases at the 3′ end were trimmed using cutadapt (1.15) and Trim Galore! (0.4.5), and the remaining reads were aligned to the mouse genome (mm10) using Bismark (0.13.1)[51] with bowtie2 (2.2.3)[52] and pbat options. UCSC genome browser[59] was used for visualizing the data.

ChIP-seq data from E16.5 male germ cells from the previous study (GSE148150)[58] were reprocessed by the following methods.[58] Briefly, reads were aligned to the mouse genome (mm10) using bwa mem (0.7.10) without options.[53] PCR duplicates and reads with low mapping quality (MAPQ <5) were removed by Picard MarkDuplicates (1.128) with the REMOVE_DUPLICATES = true option (http://broadinstitute.github.io/picard) and Samtools view (1.1) with the -q 5 option (http://www.htslib.org/), respectively. RPKM (reads per kilobase per million mapped reads) values calculated by DeepTools bamCoverage (3.0.2)[54] with -bs 100 -smoothLength 1000 –normalizeUsing RPKM options were used for visualization.

Immunohistochemistry

For immunohistochemical analysis, testes were fixed in 4% paraformaldehyde in phosphate-buffered saline (PBS) for 3 h at 4°C. Following fixation, the testes were washed three times with PBS-0.1% Triton X-(PBT) and then incubated with 10% sucrose in PBS followed by 20% sucrose in PBS for 1 h to overnight at 4°C. Subsequently, the testes were embedded in Optimum Cutting Temperature compound (Sakura Finetek 4583), following the protocol described by Hayashi et al. (2017). The embedded samples were sliced using a CM3050S cryomicrotome (Leica) to a thickness of 10 μm. The sections were permeabilized with 1% Triton X- in PBS for 15 min, blocked with 5% BSA and 1% Triton X- in PBS for 1 h, incubated with primary antibodies in 1% BSA in PBT overnight at 4°C, and subsequently incubated with secondary antibodies, followed by 5 μg/mL DAPI for 2 h at 4°C. After primary and secondary antibody treatments, the sections were washed, and the samples were mounted using Vectashield (Vector H-1000) and observed under a TCS SP8 confocal laser scanning microscope (Leica).

Single-cell fluorescence intensity was measured from two images of two optical sections with an adequate number of germ cells and somatic cells in each section, using the histogram option of LAS X software (Leica). The average intensity of the somatic cells was then calculated, and the relative signal intensity in germ cells was standardized by the average fluorescence intensity of approximately 10 surrounding somatic cells in each section. VASA-positive cells were quantified using the Analyze Particles tool in ImageJ software.

QUANTIFICATION AND STATISTICAL ANALYSIS

The statistical analyses used to evaluate the data are specified in the figure legends, accompanied by the sample size (n), denoting the number of biological replicates utilized. For RNA-seq analyses, two samples from each group were examined, whereas for all other experiments, a minimum of three samples from each group were analyzed. Unpaired two-tailed Student's *t*-tests were employed for comparisons between two groups, and one-way analysis of variance (ANOVA) with Tukey's multiple comparisons test was utilized for statistical analyses of three or more groups. Statistical significance was defined as $p < 0.05$. The following symbols are used consistently across the figures to denote statistical significance: $*p < 0.05$, $**p < 0.01$, $***p < 0.001$, and $****p < 0.0001$. All values are depicted as mean ± SEM. Statistical analyses were performed using Excel or GraphPad Prism for MacOS (GraphPad Software, Boston, Massachusetts USA).